Role of quantum confinement and hyperfine splitting in lithium-doped ZnO nanocrystals

Hyunwook Kwak
Department of Chemical Engineering and Materials Science, University of Minnesota, Minneapolis, Minnesota 55455, USA

Murilo L. Tiago* and Tzu-Liang Chan
Center for Computational Materials, Institute of Computational Engineering and Sciences, University of Texas, Austin, Texas 78712, USA

James R. Chelikowsky†,‡
Center for Computational Materials, Institute of Computational Engineering and Sciences, University of Texas, Austin, Texas 78712, USA and Departments of Physics and Chemical Engineering, University of Texas, Austin, Texas 78712, USA

(Received 15 August 2008; revised manuscript received 6 October 2008; published 24 November 2008)

The role of quantum confinement on the electronic properties of Li interstitial impurities in ZnO nanocrystals was examined using a real-space pseudopotential-density-functional method. The Li impurity was found to be partially ionized resulting in a significant charge transfer around the impurity site. To calculate the hyperfine interaction for this system using pseudopotentials, we modified Van de Walle and Blöchl's method to include explicitly the off-site contribution of the Li impurity wave function. Our modifications dramatically enhanced the agreement between the calculated and the measured isotropic hyperfine splitting constants. Our analysis with an effective-mass model demonstrates that the partial ionization of the impurity atom plays an important role both in the binding energy and in the shape of its wave function. Comparison between calculations using the local-density approximation (LDA) with LDA+U indicates that the local Coulomb correlation does not play a significant role in altering the impurity electronic states of interstitial Li-doped ZnO nanocrystals.

DOI: 10.1103/PhysRevB.78.195324 PACS number(s): 73.22.−f, 71.15.Mb, 71.55.−i, 33.15.Pw

I. INTRODUCTION

The electronic states of shallow impurities or dopants in semiconductor nanocrystals are strongly affected by the size of the nanocrystal.[1,2] Since doping changes the electronic structure significantly, a detailed knowledge of the defect electronic states is crucial in understanding the properties of the doped nanocrystals. There has been much effort to understand the physics of doped semiconductor nanocrystals both from experiment and theory. However, progress on the theoretical study of doped nanocrystals has been slow because of the large system size (typically hundreds if not thousands of atoms) and the lack of symmetry.

Here we examine the role of quantum confinement in ZnO nanocrystals. ZnO is a wide band-gap II–VI semiconductor with prospects for optoelectronic device applications.[3,4] Among many different types of doping elements for ZnO, Li has been known as one of the promising candidates for p- or n-type dopants from several bulk ZnO studies.[3,5–9] Unlike doped II–VI semiconductors such as Mn-doped CdSe,[10] Li can be more easily introduced to form a substitutional or interstitial defect in both bulk and nanocrystalline ZnO.[11]

Recently, several interesting features of Li impurities in ZnO nanoparticles have been observed from the electron-nuclear double resonance (ENDOR) spectra analysis by Orlinskii and co-workers.[12,13] Most of the Li impurities were found to form interstitial defects (Li_i), resulting in weakly bound impurity states. The measured isotropic hyperfine splitting constants (HFS) of the Li_i defects indicate a strong quantum confinement effect on the impurity states while the detailed physics remains problematic.

To understand the role of quantum confinement on the electronic properties of Li_i defects in ZnO nanocrystals, we employ a real-space first-principles pseudopotential-density-functional method. We calculate the ionization potential and the electron affinity of the undoped and Li_i-doped nanocrystals as a function of size. For doped systems, we examine the Li_i impurity state wave function to analyze its localization behavior; we found that it was not localized on the Li atom. We also predict the isotropic hyperfine splitting constant of the Li donor to assess the role of quantum confinement. We generalize Van de Walle and Blöchl's model[14] for determining the isotropic hyperfine interaction using the pseudopotential method to cases where the defect electronic states are not necessarily localized on the defect atom. We construct an effective-mass theory with a charged quantum well that provides a simple model to explain our results. To assess the role of correlation, we perform the same first-principles electronic structure calculations for several small ZnO nanocrystals with the local-density approximation (LDA)+U method and examine the role of the screened Coulomb energy on the impurity states.

II. COMPUTATIONAL DETAILS

Our calculations are based on a real-space pseudopotential-density-functional theory method.[15,16] We calculate the ground-state electronic properties of undoped and Li_i-doped ZnO nanocrystals using the LDA.[17] The total electronic energy of a system with electron density $\rho(\mathbf{r})$ can be written as

$$E_{\mathrm{tot}}[\rho(\mathbf{r})] = T[\rho(\mathbf{r})] + E_{\mathrm{ion}}[\rho(\mathbf{r})] + E_H[\rho(\mathbf{r})] + E_{xc}[\rho(\mathbf{r})], \tag{1}$$

where T is the kinetic energy, E_{ion} is the electron-ion interaction energy, E_H is the Hartree (electron-electron) energy,

and E_{xc} is the exchange-correlation energy. Minimizing the total energy based on the pseudopotential scheme gives the Kohn-Sham equation as follows:

$$\left(-\frac{\nabla^2}{2}+\sum_a V_{\text{ion}}^{\text{psp}}(\mathbf{r}-\mathbf{r}_a)+V_H[\rho(\mathbf{r})]+V_{xc}[\rho(\mathbf{r})]\right)\psi_i(\mathbf{r}) = \epsilon_i\psi_i(\mathbf{r}), \quad (2)$$

where $V_{\text{ion}}^{\text{psp}}(\mathbf{r}-\mathbf{r}_a)$ is a norm-conserving pseudopotential that replaces the Coulomb potential of each ion at $\mathbf{r}_a$, $V_H[\rho(\mathbf{r})]$ is the Hartree potential, and $V_{xc}[\rho(\mathbf{r})]$ is the exchange-correlation potential. Atomic units (a.u.) were employed throughout ($\hbar=e=m=1$). Unless stated otherwise, we use the norm-conserving pseudopotential based on Troullier and Martins.[18] The lithium pseudopotential was generated using the reference configuration $[\text{He}]2s^12p^0$ with a radial cutoff of 2.4 a.u. for the s and p channels. The oxygen pseudopotential was generated using the reference configuration $[\text{He}]2s^22p^4$ with a radial cutoff of 1.3 a.u. for both s and p channels. For LDA calculations, we considered the Zn $3d$ electrons as the core states but included partial core correction for nonlinear exchange correlation[19] in the Zn pseudopotential construction. The reference configuration for this case is $[\text{Ar}]3d^{10}4s^2$. $4p$ and $4d$ channels were also included for nonlocal component. A radial cutoff of 2.6 a.u. was chosen for all the s, p, and d channels. We tested our pseudopotentials for the ionization energy of one of our small undoped nanocrystal $[(\text{ZnO})_{17}]$. When compared with the results using zinc potential with $3d$ as valence, the difference between the two sets of results was minimal ($\lesssim$0.05 eV).

We solve the Kohn-Sham equation self-consistently on a real-space uniform grid with a higher order finite difference expression for the kinetic-energy operator.[16] The eigenvalue problem was solved by damped Chebyshev polynomial filtering subspace iteration.[20] The method distinguishes itself from the conventional diagonalization methods by avoiding computation of explicit eigenvectors except at the first self-consistent-field iteration, which speeds up the computation typically by an order of magnitude over standard diagonalization-based approaches.[20] A solution to the Kohn-Sham equation is obtained when the residual norm of the self-consistent potential is less than 10^{-4} Ry.

To model the ZnO nanocrystals, we consider spherical fragments of wurtzite structured ZnO crystal. We used the measured lattice constants of bulk wurtzite ZnO crystal: a =3.249 Å, c=5.204 Å, and c/a=1.602.[21] The surface of each nanocrystal was passivated with fictitious hydrogenlike capping atoms.[22] The capping atoms were designed to remove the surface states near the quasiparticle gap by compensating dangling bonds at the surface. For each doped nanocrystal, we placed one Li atom at the octahedral site that was nearest to the center of the nanocrystal. The structures were kept fixed in our calculations. For small nanocrystals $[(\text{ZnO})_{12}$ and $(\text{ZnO})_{17}]$, we checked that the change in the donor binding energy and the impurity HFS was less than 3% after structural relaxation.

The grid spacing for the finite difference scheme was carefully examined for convergence. We used a uniform grid spacing of 0.3 a.u.=0.016 nm. The nanocrystal of interest was placed in a spherical domain. Outside of this domain, the wave function vanishes. The domain size was chosen such that there is a vacuum space of at least 0.4 nm between the outermost atom and the domain wall.

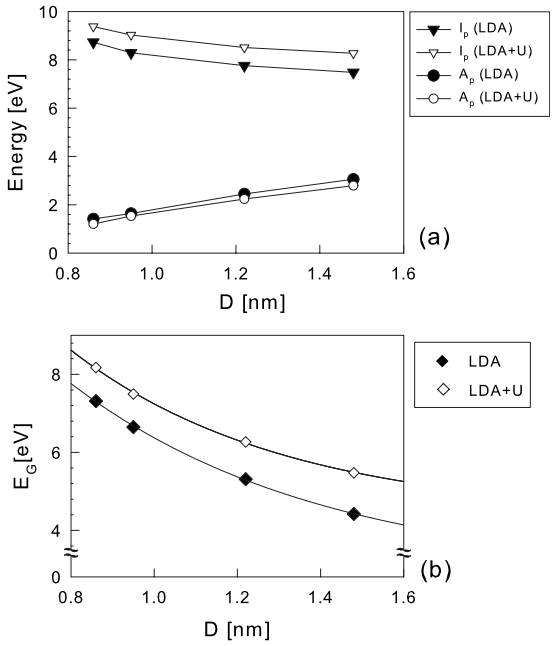

FIG. 1. Size dependence of (a) ionization energy (I_p), electron affinity (A_p), and (b) quasiparticle gap (E_g) of undoped ZnO nanocrystals. Plots with empty symbols are the results from LDA+U calculations. Solid lines in (b) are the least-squares fits to power-law functions: $4.3D^{-1.4}+2.0$ (LDA) and $4.2D^{-1.3}+3.0$ (LDA+U).

III. RESULTS

A. Electronic structure of Li_i-doped ZnO nanocrystals

Unlike the plane-wave methods with supercells, a real-space formalism allows us to calculate the ionization potential and the electron affinity of a charged, isolated system in a straightforward manner from the total-energy differences between two systems with a different number of electrons, i.e., no compensating background need to be implemented.[16] Using this method, we first investigate the ionization potential (I_p) and the electron affinity (A_p) of the undoped ZnO nanocrystals with varying sizes. The subscript p refers to a pure undoped nanocrystal. By taking the difference I_p-A_p, we obtain the quasiparticle gap (E_g) of the undoped nanocrystals, which is the energy needed to promote an electron from the highest occupied electron level to the lowest unoccupied level, assuming no interaction between the promoted electron and the residual hole that it creates.

The calculated results are shown in Fig. 1. With increasing nanocrystal size, we found that the ionization potential decreased in magnitude and the electron affinity increased. The quasiparticle gap decreases with increasing size. These trends are consistent with the previous results for semiconductor nanocrystals.[23–27] Our calculated gap scales as $\sim D^{-1.4}$ with respect to the size of the nanocrystal D. The magnitude of the scaling power is notably less than what is predicted

from an effective-mass theory ($E_g \sim D^{-2}$) (Ref. 28); however, semiconductor nanocrystals exhibit similar softness in the scaling of the energy gap.[25–27]

We also show our results using LDA+U in Fig. 1. The Zn pseudopotential for LDA+U calculations is generated with the 3d electrons treated as valence, and the reference electronic configuration is [Ar]$3d^{10}4s^2$ with 4p as an extra nonlocal component using the same radial cutoff as the LDA pseudopotential. We calculated the Hubbard U potential using first principles. The methods for calculating U for small system with inefficient screening is elaborated in our previous work.[29] Our calculated U was 6.5 eV for the smallest nanocrystal. Since the size dependence of U was weak in this size regime,[29] we applied this U value for all of our LDA+U calculations. There is a noticeable difference between LDA+U and LDA results for the ionization potential. In comparison with LDA, LDA+U gives about 1 eV larger ionization potential. As a result, the gap obtained by LDA+U was also larger than the LDA gap by ~1 eV. This can be attributed to the stronger impact of the Zn 3d level on the highest occupied states of the nanocrystal than on its lowest unoccupied state. The wave-function projection of the Zn 3d orbital onto the highest occupied energy level and the lowest unoccupied level of the undoped nanocrystals (shown in Table I) illustrates the significance of this impact.

Electron binding energy is one of the key aspects that characterize the electronic properties of impurities in semiconductors. For an n-type semiconductor, the electron binding energy provides a measure of the energy barrier to activate the electron carriers. In recent experimental studies,[12,13] Li_i defects in small ZnO nanoparticles have been labeled as shallow donors based on the partially ionized shape of the defect wave functions. However, the role of quantum confinement on the Li_i level in small ZnO nanocrystals has yet to be addressed. The Li_i defect introduces a partially occupied impurity level within the energy gap of ZnO nanocrystal. The electron binding energy E_B of this donor level can be calculated from the ionization energy (I_d) and the electron affinity (A_p) of a doped system and an undoped system, respectively:[25]

$$E_B = I_d - A_p, \tag{3}$$

where the subscript d refers to a doped ZnO nanocrystal. The calculated results are shown in Fig. 2. Clearly, the extrinsic ionization potential does not change as much with the size of a nanocrystal as the intrinsic electron affinity does. The result depicts the same picture of the pinning of an impurity level with quantum confinement observed for several other systems,[10,24–26] i.e., the impurity level does not show a sig-

TABLE I. Wave-function projections to the zinc d level of the highest occupied molecular orbital (HOMO) and the lowest unoccupied molecular orbital (LUMO) for different sizes of nanocrystals. The projections were calculated in neutral nanocrystals.

	$(ZnO)_{17}$	$(ZnO)_{38}$	$(ZnO)_{42}$	$(ZnO)_{63}$
HOMO	0.56	0.56	0.57	0.53
LUMO	0.02	0.07	0.03	0.09

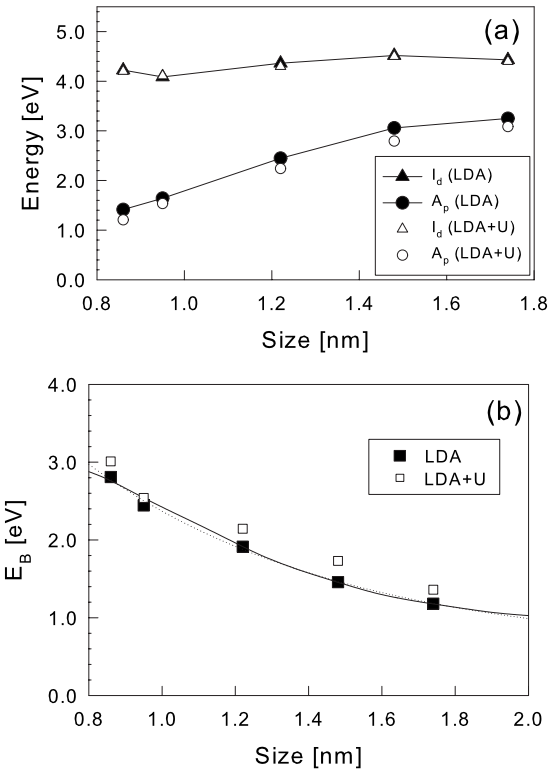

FIG. 2. Size dependence of (a) ionization energy of Li_i-doped ZnO nanocrystals (I_d), electron affinity of undoped ZnO nanocrystals (A_p), and (b) the donor-electron binding energy of Li_i-doped ZnO nanocrystals (E_B). Solid line in (b) is from our effective-mass model centered with a uniformly distributed charge. Dotted line is the least-squares fit to a power-law function $1.7D^{-1.7}+0.6$. Empty symbols are from LDA+U calculations.

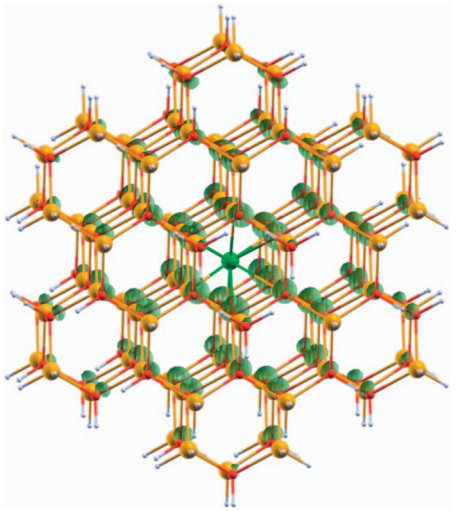

FIG. 3. (Color) Spin-density isosurface plot of the Li interstitial impurity wave function in a ZnO nanocrystal. Li atom (green sphere) is located at the octahedral site of wurtzite structured $(ZnO)_{87}$ nanocrystal. Zinc and oxygen atoms are depicted as yellow and red spheres, respectively. Small white spheres at the surface represent the capping hydrogen atoms. The green isosurface indicates electron density of the Li donor. The isosurface corresponds to 10% of the maximum value.

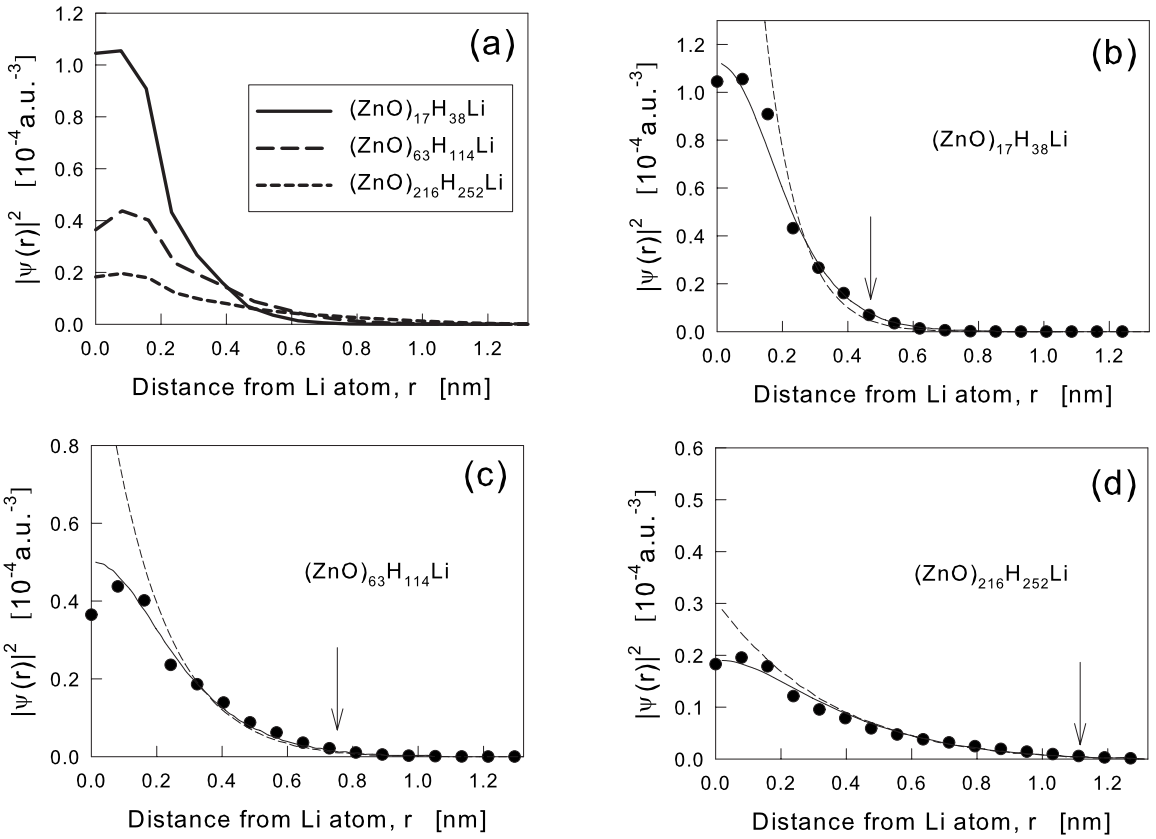

FIG. 4. (a) Spherically averaged impurity wave functions for different sizes of Li interstitial doped ZnO nanocrystals. For clarity, the wave-function profiles were averaged over a uniform radial grid of 0.06 nm. [(b)–(d)] Solid lines show the radial-wave functions from our effective-mass model. Dashed lines are from a hydrogenlike effective-mass model. Solid dots are the same spherically averaged impurity wave functions from (a). Downward arrows indicate where the surface of each nanocrystal resides.

nificant change compared to the other electronic states and is effectively pinned to the vacuum level. In addition, the electron binding energy shows a rapid increase for smaller nanocrystals. For nanocrystals with size that is less than a nanometer, the electron binding energy exceeds 2 eV. This indicates that, for a small Li_i-doped ZnO nanocrystal, the defect electronic state no longer behaves as a shallow level. From Fig. 2, the corrected energy of Zn 3*d* level by LDA $+U$ does not significantly affect the impurity level and its binding energy. Such a trivial enhancement by LDA$+U$ on the Li_i impurities in ZnO can be explained by its negligible role of the local Coulomb interaction that resides lower in the occupied states with much more contribution from the Zn 3*d* level.

B. Partial ionization of the Li impurity states

Recent experimental work[12] confirmed that the Li donor electron in a ZnO nanocrystal interacts with a large number (approximately 20) of its neighboring atoms. In contrast, the defect wave functions of phosphorus substitutional defect in Si nanocrystals were sharply localized at the impurity atom site.[25,26,30] The nature of Li_i defects in ZnO nanocrystals should be very different from that of P in Si nanocrystals.

In Fig. 3, we plotted an isosurface of the electron density of the defect wave function for $(ZnO)_{87}LiH_{126}$. The defect wave function was not localized on the Li atom, and was distributed on its neighbors. This is consistent with the experimental observation that the donor interacts with a large number of surrounding atoms.[12] Figure 4(a) shows the defect wave functions for different sizes of ZnO nanocrystals. The wave functions were spherically averaged to illustrate the decay from the Li atom. We smooth the wave functions by averaging them within a radial grid of 0.06 nm. From the figure, the partially ionized feature of the Li_i donors can be seen from the maximum located on the neighboring sites rather than the impurity site. The figure also illustrates a strong size effect on the impurity wave function. As the size increases, the defect wave function becomes more spatially extended. Our result is consistent with the binding energy of Li_i donors in ZnO being close to zero in the bulk limit.[12] The delocalized feature of the defect wave function can also be found in Li_i-doped Si nanocrystals.[31]

As the donor electron becomes significantly delocalized from the Li atom, the nanocrystal will compensate the positive charge of the Li ion by transferring electrons toward the impurity atom site. To illustrate this, we calculated the atom-site-projected charge densities for both pure and doped nanocrystals, and examined the difference. The projected charge density for each atom site was estimated within the covalent radius of each atom type. The difference in charge density between doped and undoped $(ZnO)_{42}H_{72}$ for each atom site is depicted in Fig. 5.

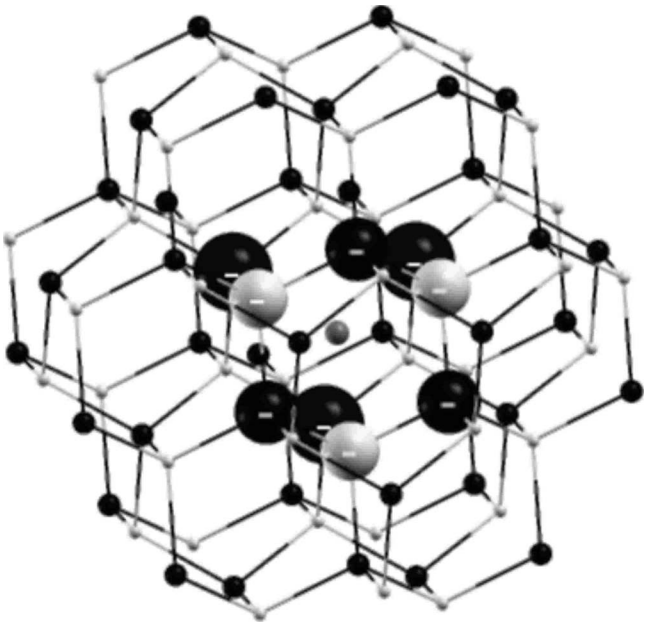

FIG. 5. Charge transfer around the Li interstitial atom (gray sphere) in $(ZnO)_{42}$–Li nanocrystal. Zinc and oxygen atoms are depicted as black and white spheres, respectively. If electrons are transferred toward an atom, the atom is labeled with the (–) sign. For all other atoms, electrons are transferred out of them. The capping-layer atoms are not shown for clarity. The size of each sphere denotes the magnitude of charge transfer.

There is a noticeable electron transfer toward the defect atom site caused by the Li_i defect. The nearest-neighbor gains $0.04e-0.08e$ of charge per atom for Zn and $0.006e-0.02e$ of charge per atom for O. As a reaction to the charge transfer toward the first neighbor of the impurity site, each atom in the outer region slightly loses its charge by $\leq 0.02e$ for Zn and $\leq 0.001e$ for O.

C. Isotropic hyperfine splitting constant

Orlinskii and co-workers[12,13] have shown strong quantum confinement effect on the defect wave function by measuring the isotropic HFS of Li-doped ZnO nanocrystals. Since HFS scales with the contact interaction between the electron and the nuclei, it is a useful indicator of how quantum confinement affects the electronic states under quantum confinement.[2,25,32]

The isotropic hyperfine parameter a_{iso} of a wave function can be written as

$$a_{\mathrm{iso}} = \frac{8\pi}{3} g_e \beta_e g_n \beta_n s(\mathbf{0}). \tag{4}$$

Here, g_e is the electron g factor, g_n is the g factor of the nucleus, β_e is the electronic Bohr magneton, β_n is the nuclear magneton, and $s(\mathbf{0})$ is the spin density at the nucleus site. Since the spin density of a Li-doped ZnO crystal is equal to the amplitude square of the Li donor wave function $[s(\mathbf{0}) = |\psi(\mathbf{0})|^2]$, the isotropic HFS of Li donor can be calculated given the defect wave function.

Since the pseudopotential approach implies a modification of the wave function inside the core radius of each atom, the approach is not appropriate for a detailed description of the atom core region, including the isotropic HFS. Van de Walle and Blöchl[14] suggested a scheme that enables us to estimate the isotropic HFS from the pseudopotential calculations. In this scheme, the all-electron impurity wave function $|\psi\rangle$ is written as a linear combination of the corresponding pseudowave function $|\tilde{\psi}\rangle$ and pseudoatomic wave functions $|\tilde{\phi}_l\rangle$ of atoms in the system:

$$|\psi\rangle = |\tilde{\psi}\rangle + \sum_l (|\phi_l\rangle - |\tilde{\phi}_l\rangle)\langle\tilde{\phi}_l|\tilde{\psi}\rangle, \tag{5}$$

where $|\phi_l\rangle$ is the all-electron atomic wave function. The index l runs over each and every atom site and the angular-momentum component. Since the pseudowave functions are constructed to be the same as the all-electron wave functions outside the core radius of an atom, the wave-function value at the impurity site can be written as

$$\psi(\mathbf{0}) = \tilde{\psi}(\mathbf{0}) + \langle\tilde{\phi}_s|\tilde{\psi}\rangle[\phi_s(\mathbf{0}) - \tilde{\phi}_s(\mathbf{0})], \tag{6}$$

where the index s represents the s component of the impurity atom. While the all-electron and pseudoatomic wave functions $[\phi_s(\mathbf{0})]$ and the pseudoimpurity wave function $[\tilde{\psi}(\mathbf{0})]$ can be calculated from first principles, the integral $\langle\tilde{\phi}_s|\tilde{\psi}\rangle$ cannot be evaluated easily. However, one can derive an estimate of the integral by expressing the pseudowave function as an expansion of the pseudoatomic wave functions $|\tilde{\psi}\rangle = \Sigma_l\langle\tilde{\phi}_l|\tilde{\psi}\rangle|\tilde{\phi}_l\rangle$. The value of the pseudoimpurity wave function at the impurity atom can then be written as

$$\tilde{\psi}(\mathbf{0}) = \langle\tilde{\phi}_s|\tilde{\psi}\rangle\tilde{\phi}_s(\mathbf{0}) + \sum_{l\neq s}\langle\tilde{\phi}_l|\tilde{\psi}\rangle\tilde{\phi}_l(\mathbf{0}). \tag{7}$$

Van de Walle and Blöchl[14] postulated that, for a localized defect state, only the defect atomic orbitals contribute to the defect state wave function. With this postulate, only the term with the defect s orbital remains nonzero and Eq. (7) becomes

$$\tilde{\psi}(\mathbf{0}) = \langle\tilde{\phi}_s|\tilde{\psi}\rangle\tilde{\phi}_s(\mathbf{0}), \tag{8}$$

or

$$\langle\tilde{\phi}_s|\tilde{\psi}\rangle = \frac{\tilde{\psi}(\mathbf{0})}{\tilde{\phi}_s(\mathbf{0})}. \tag{9}$$

Therefore, Eq. (6) can be simply written as

$$\psi(\mathbf{0}) = \tilde{\psi}(\mathbf{0})\frac{\phi_s(\mathbf{0})}{\tilde{\phi}_s(\mathbf{0})}. \tag{10}$$

Based on this simple expression, pseudopotential calculations for the HFS of P-doped Si nanocrystals are in excellent agreement with the experimental observations.[25,26] However, the Van de Walle-Blöchl postulate that the defect atomic orbital solely contributes to the defect wave function will not hold for partially ionized defects.[33]

If one does not neglect the off-site contributions to the defect state from Eq. (7), Eq. (9) should be rewritten as

$$\langle \tilde{\phi}_s | \tilde{\psi} \rangle = \frac{1}{\tilde{\phi}_s(\mathbf{0})} \left[\tilde{\psi}(\mathbf{0}) - \sum_{l \neq s} \langle \tilde{\phi}_l | \tilde{\psi} \rangle \tilde{\phi}_l(\mathbf{0}) \right], \tag{11}$$

Putting this expression to Eq. (6) gives

$$\psi(\mathbf{0}) = \tilde{\psi}(\mathbf{0}) + \left(\frac{\phi_s(\mathbf{0})}{\tilde{\phi}_s(\mathbf{0})} - 1 \right) \left[\tilde{\psi}(\mathbf{0}) - \sum_{l \neq s} \langle \tilde{\phi}_l | \tilde{\psi} \rangle \tilde{\phi}_l(\mathbf{0}) \right]. \tag{12}$$

By defining $\tilde{\mu} \equiv \Sigma_{l \neq s} \langle \tilde{\phi}_l | \tilde{\psi} \rangle \tilde{\phi}_l(\mathbf{0}) / \tilde{\psi}(\mathbf{0})$, the equation is reduced to a simple expression:[34]

$$\psi(\mathbf{0}) = \tilde{\psi}(\mathbf{0}) \left[\frac{\phi_s(\mathbf{0})}{\tilde{\phi}_s(\mathbf{0})} (1 - \tilde{\mu}) + \tilde{\mu} \right]. \tag{13}$$

The impurity wave function consists of contributions from the defect atom as well as all the other atoms in the system. In fact, Van de Walle-Blöchl method corresponds to one of the limiting cases where $\tilde{\mu}=0$ and therefore only the defect on-site term is relevant, i.e., a defect state sharply localized at the defect atom. For a nearly ionized impurity, $\langle \tilde{\psi} | \tilde{\phi}_s \rangle$ is small and therefore the dominant contribution to $\psi(\mathbf{0})$ is from the neighboring atoms. For such a case, $\tilde{\mu}$ should be close to one. In general, $\tilde{\mu}$ can be interpreted as a measure of the off-site contribution to the HFS.

Although the evaluation of $\tilde{\mu}$ requires the defect wave function to be expressed in terms of a localized basis set $|\tilde{\phi}_l\rangle$, direct evaluation of $\tilde{\mu}$ can be avoided. $\tilde{\mu}\tilde{\psi}(\mathbf{0}) = \Sigma_{l \neq s} \langle \tilde{\phi}_l | \tilde{\psi} \rangle \tilde{\phi}_l(\mathbf{0})$ should depend very weakly on the core structure of the Li s state or the choice of the pseudopotential within the core region. Based on this observation, $\tilde{\mu}$ can be calculated by performing two separate calculations with different types of pseudopotentials. Both calculations should give the same physical result, and therefore the same HFS. Using Eq. (12),

$$\tilde{\psi}(\mathbf{0}) + (u-1)[\tilde{\psi}(\mathbf{0}) - \tilde{\mu}\tilde{\psi}(\mathbf{0})] = \tilde{\psi}'(\mathbf{0}) + (u'-1)[\tilde{\psi}'(\mathbf{0}) - \tilde{\mu}\tilde{\psi}(\mathbf{0})], \tag{14}$$

where $\tilde{u} = \phi_s(\mathbf{0}) / \tilde{\phi}_s(\mathbf{0})$, and the prime indicates values calculated using a second pseudopotential. $\tilde{\mu}$ can then be solved resulting in the following expression:

$$\tilde{\mu} = \frac{\tilde{u} - \left(\frac{\tilde{\psi}'(\mathbf{0})}{\tilde{\psi}(\mathbf{0})} \right) \tilde{u}'}{\tilde{u} - \tilde{u}'}. \tag{15}$$

We used Troullier-Martins[18] (TM) and Bachelet-Hamann-Schlüter (BHS) (Refs. 35 and 36) pseudopotentials for Li to calculate $\tilde{\mu}$ for five of our small nanocrystals. The BHS Li pseudopotential was generated using the same reference configuration as the TM pseudopotential but the radial cutoff was set to be 2.0 a.u. Our calculated $\tilde{\mu}$ are shown in Table II. The values were close to 0.8 and were insensitive to size. This is consistent with our description of the Li donor state in the previous section because the system is close to one of the limiting cases where $\tilde{\mu}$ is one and the impurity atom is completely ionized.

TABLE II. The off-impurity site contribution $\tilde{\mu}$ of the hyperfine interaction at the defect (Li_i) site for different sizes of the doped ZnO nanocrystals.

	$(ZnO)_{17}$	$(ZnO)_{38}$	$(ZnO)_{45}$	$(ZnO)_{63}$	Avg.
μ	0.82	0.84	0.84	0.83	0.83

Using $\tilde{\mu}=0.83$ in Eqs. (4) and (13), our calculated HFS were plotted with experimental results from Orlinskii *et al.*[13] in Fig. 6. Results from Van de Walle-Blöchl method ($\mu=0$) was also plotted. Predictions based on Van de Walle-Blöchl method were off by almost two orders of magnitudes from the experiment while our results can be extrapolated to experimental data smoothly where it scales as D^{-3} for larger nanocrystals ($D>3$ nm). The agreement between theory and experiment would be dramatically improved if off-site contributions are considered. HFS calculated using the LDA $+U$ method are also plotted in Fig. 6, and we found that the change in the Li HFS caused by the U potential is minimal.

The D^{-3} dependence in the larger systems implies that they can be modeled as an infinite-depth quantum well in an effective-mass theory.[28] However our calculated HFS size dependence changes slowly from D^{-3} for diameters larger than ~ 3 nm to $\approx D^{-1.6}$ for smaller nanocrystals. The softer size dependence in smaller systems cannot be understood with such theory.

IV. DISCUSSION

To gain further insight of our results on Li_i-doped ZnO nanocrystals, we constructed a quantum-well model based on effective-mass theory. Our model was based on a potential well with radius R and depth V_0 with a dielectric constant of ϵ. Instead of placing a point charge at the center to mimic the Li ion, we placed a uniformly charged core with radius R' and charge density $\rho = 3/(4\pi R'^3)$. This was motivated by our

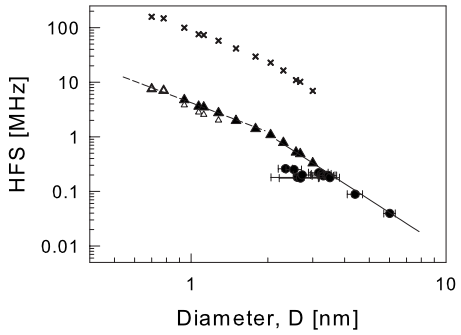

FIG. 6. Log scale plot of the isotropic hyperfine splitting constant of Li_i-doped ZnO nanocrystals as a function of nanocrystal size. Theoretical results with LDA are plotted as filled triangles while results from LDA$+U$ are plotted as empty triangles. Experimental data plotted as circles with error bars was taken from the most recent ENDOR analysis by Orlinskii *et al.* (Ref. 13). Theoretical results from Van de Walle-Blöchl method is plotted as ×'s. Solid line depicts the scaling of $\sim D^{-3}$ for larger nanocrystals and dashed line depicts the scaling of $\sim D^{-1.6}$ for smaller nanocrystals.

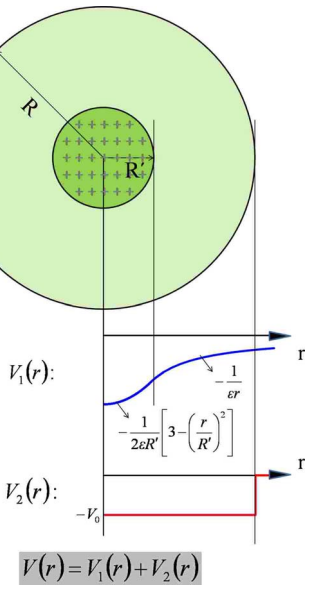

FIG. 7. (Color online) An illustration of our effective-mass model with a uniformly distributed charge in a quantum well and the potential profile $V(r)$ with the distance r from its center. Radius and depth of the spherical potential well are R and V_0, respectively. Positive charge at the center is distributed uniformly over a small sphere of radius R'. The quantum well also has a dielectric constant ε.

calculation results which indicate that the impurity wave function has a maximum that is not on the Li position but is dispersed near the Li position.

Figure 7 illustrates our effective-mass model with a uniformly distributed charge as its core. One can construct a model Hamiltonian $\hat{H}=(-\nabla^2/2m^*)+V(r)$ (in atomic units) for an electron with an effective mass m^* and a radial potential function $V(r)$ with respect to the distance r from the impurity site at the origin,

$$V(r)=\begin{cases}-\dfrac{1}{2\epsilon R'}\left[3-\left(\dfrac{r}{R'}\right)^2\right]-V_0 & \text{if } 0<r\leq R',\\ -\dfrac{1}{\epsilon r}-V_0 & \text{if } R'<r\leq R,\\ -\dfrac{1}{\epsilon r} & \text{if } r>R.\end{cases} \tag{16}$$

From Figs. 3 and 5, it is clear that the maximum of the impurity wave function occurs around the nearest neighbor of the impurity atom. Therefore, it is reasonable to set the charged core radius as the distance between Li and its nearest-neighbor atoms ($R'=0.2$ nm). For the effective mass, we used the bulk ZnO value ($m^*=0.28$).[21] We applied the generalized Penn's model[37,38] for the size dependence of the dielectric constant:

$$\epsilon(D)=1+\frac{\epsilon_b-1}{1+\left(\dfrac{\alpha}{D}\right)^n}, \tag{17}$$

where ϵ_b is the static dielectric constant of bulk ZnO ($\epsilon_b=8.65$),[21] and α and n will be used as fitting parameters.

By solving the Schrödinger equation $\hat{H}\psi(r)=E\psi(r)$ numerically, we obtained the ground-state wave function and the ground-state eigenvalue which correspond to the impurity wave function and the donor binding energy, respectively. We adjusted α, n, and V_0 in our effective-mass model to fit the binding energies and the shape of the impurity wave functions to our pseudopotential-density-functional theory results. We found a set of parameters: $\alpha=1.2$ nm, $n=3.5$, and $V_0=1.1$ eV to be the best fit. In Figs. 4(b)–4(d), ground-state wave functions from the effective-mass model with different well radii are plotted with each of the corresponding spherically averaged wave functions from the pseudopotential calculations. In Fig. 2, the size dependence of the binding energy from the effective-mass model agrees well with the pseudopotential work. The scaling of the donor binding energy in Fig. 2 ($E_B\sim D^{-1.7}$) can be understood as a mixture of Coulomb interaction ($\sim D^{-1}$) and kinetic-energy contribution ($\sim D^{-2}$) owing to quantum confinement. This indicates that the role of the Coulomb interaction between the donor electron and the impurity atom, and the role of spatial confinement are equally important to the Li_i donor's behavior.

To clarify the role of the uniformly charged core in our effective-mass model, we constructed a similar quantum well with a point charge instead of a uniform charge distribution, and performed the same analysis. Dashed lines in Figs. 4(b)–4(d) show the form of the impurity wave function for the hydrogen-in-a-quantum-well effective-mass model. The results were calculated with the set of parameters ($\alpha=1.3$ nm and $n=2.7$) that best fit the binding energy from the pseudopotential calculations. Its exponential trend near the origin does not agree with the qualitative feature of the Li donor wave function near the impurity site. This trend reinforces the importance of our modification of the model near the impurity site that describes the partially ionized impurities under quantum confinement.

Our effective-mass model also helps us to understand the softer size dependence of Li HFS for small nanocrystals shown in Fig. 6. When a doped nanocrystal is sufficiently large ($R'\ll R$), the impurity nucleus will simply act like a point charge. However, when the size of the nanocrystal is comparable to the size of the ionic core in our effective-mass model, the scaling behavior of the hyperfine interaction will deviate from what is expected from a hydrogenlike effective-mass model, resulting in a gradual change in the scaling of the HFS. Our analysis discloses that, owing to the partially ionized nature of the Li_i defect in ZnO nanocrystals, the defect state and its binding energy cannot be described by a traditional hydrogenlike effective-mass theory.

V. CONCLUSIONS

We examined the role of quantum confinement on the electronic properties of Li_i impurities in ZnO nanocrystals

with a real-space pseudopotential method. By calculating the total energy of ZnO nanocrystals with different sizes, we found that the ionization potential and the electron affinity of undoped ZnO nanocrystals show a strong size dependence. The scaling of the energy gap of ZnO nanocrystals were similar to that of other semiconductor nanocrystals. For doped systems, we found that the ionization potential of Li_i-doped ZnO nanocrystals is virtually independent of size. The electron binding energy of Li donor shows a rapid increase as the size decreases. We compared our calculation results with LDA+U to examine the role of screened local Coulomb energy. We found that LDA+U properly corrects the energy level of locally correlated states; however the enhancement becomes much less relevant for the impurity states.

The Li_i impurity state wave function was plotted and analyzed to study its localization behavior. We found that the Li impurity partially ionizes and triggers a charge redistribution around the impurity site. From our study of the size dependence of Li HFS, we also found that the partial ionization demands modifications in Van de Walle and Blöchl's method to calculate the hyperfine interactions using pseudopotentials. Our modification of the method can describe the off-site contribution to the HFS, and our calculated HFS can be extrapolated to the experimental data smoothly.

We also examined our calculation results with an effective-mass model. The model was designed to simulate the partially ionized impurity site with a small, uniformly charged sphere at the center of a quantum well. With a proper parametrization, the model successfully described the shape of the impurity wave function as well as the size dependence of the binding energy. Our analysis points out that the partial ionization of the impurity plays an important role in the electronic properties of Li_i-doped ZnO nanocrystals.

ACKNOWLEDGMENTS

This work has been supported in part by the National Science Foundation under Contract No. DMR-0551195, and the U.S. Department of Energy under Contracts No. DE-FG02-06ER15760 and No. DE-FG02-06ER46286. Calculations were performed at the Texas Advanced Computing Center (TACC). We thank S. P. Beckman and A. Zayak for helpful discussions.

*Present address: Materials Science and Technology Division, Oak Ridge National Laboratory, Oak Ridge, TN 37831, USA
†Corresponding author
‡jrc@ices.utexas.edu

[1] A. D. Yoffe, Adv. Phys. **50**, 1 (2001).
[2] M. Fujii, A. Mimura, S. Hayashi, Y. Yamamoto, and K. Murakami, Phys. Rev. Lett. **89**, 206805 (2002).
[3] O. Lopatiuk, L. Chernyak, A. Osinsky, and J. Q. Xie, Appl. Phys. Lett. **87**, 214110 (2005).
[4] D. Karmakar, S. K. Mandal, R. M. Kadam, P. L. Paulose, A. K. Rajarajan, T. K. Nath, A. K. Das, I. Dasgupta, and G. P. Das, Phys. Rev. B **75**, 144404 (2007).
[5] C. H. Park, S. B. Zhang, and S.-H. Wei, Phys. Rev. B **66**, 073202 (2002).
[6] J. G. Lu *et al.*, Appl. Phys. Lett. **89**, 112113 (2006).
[7] M. G. Wardle, J. P. Goss, and P. R. Briddon, Phys. Rev. B **71**, 155205 (2005).
[8] E. C. Lee and K. J. Chang, Phys. Rev. B **70**, 115210 (2004).
[9] Y. J. Zeng, Z. Z. Ye, J. G. Lu, W. Z. Xu, L. P. Zhu, and B. H. Zhao, Appl. Phys. Lett. **89**, 042106 (2006).
[10] G. M. Dalpian and J. R. Chelikowsky, Phys. Rev. Lett. **96**, 226802 (2006).
[11] A. Onodera, K. Yoshino, H. Satoh, H. Yamashita, and N. Sakagami, Jpn. J. Appl. Phys., Part 1 **37**, 5315 (1998).
[12] S. B. Orlinskii, J. Schmidt, P. G. Baranov, D. M. Hofmann, C. de Mello Donegá, and A. Meijerink, Phys. Rev. Lett. **92**, 047603 (2004).
[13] S. B. Orlinskii, J. Schmidt, E. J. J. Groenen, P. G. Baranov, C. de Mello Donegá, and A. Meijerink, Phys. Rev. Lett. **94**, 097602 (2005).
[14] C. G. Van de Walle and P. E. Blöchl, Phys. Rev. B **47**, 4244 (1993).
[15] J. R. Chelikowsky, N. Troullier, and Y. Saad, Phys. Rev. Lett. **72**, 1240 (1994).
[16] J. R. Chelikowsky, J. Phys. D **33**, R33 (2000).
[17] W. Kohn and L. J. Sham, Phys. Rev. **140**, A1133 (1965).
[18] N. Troullier and J. L. Martins, Phys. Rev. B **43**, 1993 (1991).
[19] S. G. Louie, S. Froyen, and M. L. Cohen, Phys. Rev. B **26**, 1738 (1982).
[20] Y. Zhou, Y. Saad, M. L. Tiago, and J. R. Chelikowsky, Phys. Rev. E **74**, 066704 (2006).
[21] O. Madelung, *Semiconductors: Data Handbook*, 3rd ed. (Springer, New York, 2004).
[22] X. Huang, E. Lindgren, and J. R. Chelikowsky, Phys. Rev. B **71**, 165328 (2005).
[23] E. Meulenkamp, J. Phys. Chem. B **102**, 5566 (1998).
[24] M. M. G. Alemany, X. Y. Huang, L. J. G. M. L. Tiago, and J. R. Chelikowsky, Nano Lett. **7**, 1878 (2007).
[25] D. V. Melnikov and J. R. Chelikowsky, Phys. Rev. Lett. **92**, 046802 (2004).
[26] T. L. Chan, M. L. Tiago, and J. R. Chelikowsky, Nano Lett. **8**, 596 (2008).
[27] M. Lopez del Puerto, M. L. Tiago, and J. R. Chelikowsky, Phys. Rev. B **77**, 045404 (2008).
[28] L. E. Brus, J. Chem. Phys. **79**, 5566 (1983).
[29] H. Kwak, M. L. Tiago, and J. R. Chelikowsky, Solid State Commun. **145**, 227 (2008).
[30] Z. Y. Zhou, M. L. Steigerwald, R. A. Friesner, L. Brus, and M. S. Hybertsen, Phys. Rev. B **71**, 245308 (2005).
[31] H. Kwak, T. L. Chan, and J. R. Chelikowsky (unpublished).
[32] G. Feher, Phys. Rev. **114**, 1219 (1959).
[33] H. Kwak, M. L. Tiago, T. L. Chan, and J. R. Chelikowsky, Chem. Phys. Lett. **145**, 227 (2008).
[34] In our previous report (Ref. 33), the off-site contribution was added to the pseudocharge density rather than the pseudowave

function. This is not correct in general. However, all our previous results are still qualitatively correct.

[35] D. R. Hamann, M. Schlüter, and C. Chiang, Phys. Rev. Lett. **43**, 1494 (1979).

[36] G. B. Bachelet, D. R. Hamann, and M. Schlüter, Phys. Rev. B **26**, 4199 (1982).

[37] D. R. Penn, Phys. Rev. **128**, 2093 (1962).

[38] A. C. Sharma, J. Appl. Phys. **100**, 084301 (2006).